

## Article

# Research on the Thermal Stability in High-Temperature Air of Cr-Fe Composite Oxide Solar Coatings by Chemical-Colored of Stainless Steel

Hongwen Yu <sup>1,2,\*</sup> , Yi He <sup>2</sup>, Ziyi Song <sup>2</sup>, Xinyu Zhang <sup>1,\*</sup>, Yibing Xue <sup>2,\*</sup> and Lei Feng <sup>3</sup>

<sup>1</sup> State Key Laboratory of Building Safety and Environment & National Engineering Research Center of Building Technology, Beijing 100013, China

<sup>2</sup> The School of Architecture and Urban Planning, Shandong Jianzhu University, Jinan 250101, China

<sup>3</sup> Shandong Sangle Group Co., Ltd., Jinan 250101, China

\* Correspondence: hongwen\_yu@163.com (H.Y.); zxyhit@163.com (X.Z.); xueyb@sdjzu.edu.cn (Y.X.)

**Abstract:** The stainless steel chemical coloration demonstrates excellent repeatability of process when adopted to fabricate solar selective absorber coatings (SSACs) on TTS445J1 stainless steel base material. The optical performance, morphology, and composition of coatings are characterized by UV-3600, IR-Affinity-1, SEM, EDS, etc. The experimental results suggest that the Cr-Fe composite oxides with coatings in a spinel structure obtained by chemical coloration on a stainless steel surface exhibit outstanding spectral selectivity, with  $\alpha/\varepsilon = 0.9334/0.1326$ . The coatings were generated by the direct reaction between the stainless steel substrate composition and the coloring solution, which changes the traditional way of combining the coating with the substrate by physical methods. Comparing the SEM images of the coatings before and after aging at 500 °C in air, we noticed no significant changes at the interface between the coatings and the substrate, indicating excellent coating adhesion. At the same time, the substrate grains did not change much after the chemical reaction of the stainless steel substrate, indicating that the oxidation resistance of the stainless steel substrate was not weakened. Finally, the Cr-Fe composite oxide exhibited excellent thermal stability in air. Based upon a microstructure analysis, the Performance Creation (*PC*) is 0.01 after aging at 500 °C for 200 h in high-temperature air, primarily because of the loss of H<sub>2</sub>O molecules from the hydrates in the coatings. After aging for 800 h, *PC* = 0.0458. After the aging hours are extended to 1000 h, *PC* = 0.0762. During the aging process at high temperature, the coatings of the Cr-Fe composite oxides maintained stable composition and phase structures. The decay in optical performance is due mainly to the reconstruction of the surface morphology of the coatings as a result of the enlarging of grains.

**Keywords:** chemical-colored of stainless steel; Cr-Fe composite oxide; SSACs; thermal stability



**Citation:** Yu, H.; He, Y.; Song, Z.; Zhang, X.; Xue, Y.; Feng, L. Research on the Thermal Stability in High-Temperature Air of Cr-Fe Composite Oxide Solar Coatings by Chemical-Colored of Stainless Steel. *Processes* **2023**, *11*, 213. <https://doi.org/10.3390/pr11010213>

Academic Editors: Pedro Dinis Gaspar, Pedro Dinho da Silva and Luis C. Pires

Received: 20 December 2022

Revised: 5 January 2023

Accepted: 6 January 2023

Published: 9 January 2023



**Copyright:** © 2023 by the authors. Licensee MDPI, Basel, Switzerland. This article is an open access article distributed under the terms and conditions of the Creative Commons Attribution (CC BY) license (<https://creativecommons.org/licenses/by/4.0/>).

## 1. Introduction

The medium temperatures (working temperature range 100~250 °C) [1] in solar heat utilization are mainly applied in domains of heat for industrial and agricultural purposes [2], which, according to statistics, will be three to five [3] times the market size of low-temperature utilization. As a medium-to-high-temperature photothermal base material, stainless steel [4] is typically adopted in lieu of traditional base materials of copper and aluminum. There are two major solutions to the heat collection structure in medium-to-high-temperature solar heat utilization: One is the metal-glass vacuum tube [5] heat collection structure, with photothermal conversion coatings in the vacuum environment; the other is developing a solar thermal collector working under atmospheric conditions [6] by light-converging means. The metal-glass vacuum tube heat collection structure is a relatively maturely commercialized technique. However, such metal-glass vacuum tubes have high manufacturing costs [5,7] and are also easy to damage, thereby leading to the loss of vacuum degree and affecting heat-collecting efficiency. Relative to the heat collection

method under vacuum conditions, the solar heat collection technology operating in the atmosphere [8] is easy to implement (for saving the high costs of metal-glass vacuum heat collectors), though it presents higher requirements on solar selective absorber coatings (SSACs), the core of photothermal conversion. SSACs, when working in a high-temperature environment in the atmosphere, increase the probability that chemical or physical degradation [9] occurs. This phenomenon stems mainly from the fact that such coatings are prone to unstable behaviors, such as agglomeration, growing, oxidation, and interlayer atomic migration by diffusion [10], in a high-temperature oxygen environment. Such unstable behaviors could cause changes in the composition and microstructure of coatings [5]. These unstable behaviors can lead to changes in the coatings composition and microstructure, resulting in the degradation of the optical properties of the coatings. These phenomena of coatings degradation could have immediate [11], lethal effects on the optical performance of coatings.

The ideal SSACs [12] has high solar absorptance ( $\alpha > 90\%$ ) while maintaining low thermal emittance ( $\varepsilon < 20\%$ ) at working temperature. By Chinese energy industry standard “Durability Specification for Absorber of Flat Plate Solar Collect” (NB/T 34072-2018), weatherability of SSACs is rated as  $PC \leq 0.05$  by the following definition:

$$PC = -\Delta\alpha + 0.5\Delta\varepsilon \quad (1)$$

where  $PC$ ,  $\Delta\alpha$  and  $\Delta\varepsilon$  denote the Performance Creation and the absolute values of change of  $\alpha$  and  $\varepsilon$  before and after experiment, respectively.

Over the recent decade, the medium-temperature SSACs [12] coatings which are applicable in air have received considerable attentions of researchers. There are many methods to fabricate SSACs, such as deposition (physical vapor deposition (PVD) [13], chemical vapor deposition (CVD) [14], etc.), wet chemical deposition (sol-gel dip coating [15], electrochemical deposition [16], etc.), etc. The commonly used commercially available SSACs are prepared by PVD because of their outstanding optical properties. However, the relatively high equipment investment cost, limited coating area and the inconvenience of fabrication on complex surfaces hinder its large-scale application. In contrast, wet chemical deposition shows great promise as an economical, simple, and reproducible method for the fabrication of SSACs.

The thermal stability of the coatings has been affected by three main reasons [11,17]. First, the coating materials have thermal stability and oxidation resistance. Second, the substrate materials have good bonding properties with the coatings. Finally, the substrate materials have strong oxidation resistance. In the process of high temperature aging, the coefficient of thermal expansion of substrate and coatings is not consistent, repeated thermal expansion and contraction process, the coatings will produce cracks and even peel off. In terms of materials, spinel materials have characteristic high temperature stability against air corrosion, such as transition metal complex oxides, metal oxides, nitrides, etc., making them a suitable candidate as SSACs. Al-Rjoub et al. [17] reported the stability of W/WSiAlN<sub>x</sub>/WSiAlO<sub>y</sub>N<sub>x</sub>/SiAlO<sub>x</sub> at 400 °C and at 600 °C in air and in vacuum, respectively. Lee et al. [8] reported a CrAlSiN-based nanometer multilayer solar selective coatings composed of polycrystalline CrN and amorphous AlSiN and conducted an oxidation behavior test for 100 h in air within a temperature range of 800~1000 °C. Liu et al. [15] reported a TiAlON-based nanometer multilayer coatings, whose solar selectivity was 0.936/0.17 with a slight variation of 0.922/0.175 and which was stabilized for 50 h in 550 °C air. Juan F. Torres et al. [18] reported Al and Ti-SiO<sub>2</sub> coralloid coatings, which exhibited ultrahigh stability after being aged in high-temperature ( $\geq 800$  °C) air for over 2000 h. Beibei Lu et al. [9] fabricated a composite coatings of Si<sub>3</sub>N<sub>4</sub>, a-Si, Ag, and Cr<sub>2</sub>O<sub>3</sub>, which showed no obvious interfacial diffusion after being annealed at 400 °C in air. Hao Wang et al. [19] designed a SiO<sub>2</sub>-Si<sub>3</sub>N<sub>4</sub>-W-SiO<sub>2</sub>-W coatings, which remained stable after being heated for 72 h at 400 °C in air.

In the last decade, the wet chemical preparation of spinel materials has attracted great attention in order to solve the problem of thermal stability of SSACs in air. Zhiyan

Yang [10] prepared  $\text{Ni}_9\text{Fe}_1\text{Co}_2\text{O}_y$  by sol-gel spraying, was heated continuously at  $500\text{ }^\circ\text{C}$  for 48 h in air and the solar absorptance remained at 0.93. M. Shiva Prasad [20] prepared a series of composite nanoparticles  $\text{Mn-Cu-Co-O}_x\text{-ZrO}_2/\text{MgF}_2$  by sol-gel method and dipped on stainless steel substrates, which achieved  $\alpha/\varepsilon = 0.97/0.17$  at  $500\text{ }^\circ\text{C}$ . Atchuta [21] prepared transition metal nitrate precursors to obtain  $\text{Cu}_x\text{Ni}_y\text{Co}_{z-x-y}\text{O}_4$  spinel solar selective absorption coatings and deposited on austenitic stainless steel substrates with spectral selectivity of  $\alpha/\varepsilon = 0.91/0.14$ .

Possessing very high corrosion resistance and excellent thermal stability [22] at high temperature, as well as semiconductive properties [8], Cr and Fe oxides are common materials for SSACs. Coatings obtained by stainless steel chemical coloration are exactly the Cr-Fe oxidated compounds [23], which is the theoretical basis for preparing solar coatings by stainless steel chemical coloration. In the past, the substrate and the coatings were two separate materials that were combined by physical means. PVD and CVD generally adds a layer of metal deposition to enhance the adhesion of the coatings. Wet chemical deposition generally adopts the method of coatings colloidal solution on the surface of the substrate and finally high temperature curing to improve the adhesion of the coatings. In this work, we performed chemical-colored at a reaction temperature of  $118\text{ }^\circ\text{C}$ , with TTS445J1 stainless steel as the base material and  $\text{Na}_2\text{Cr}_2\text{O}_7\text{-H}_2\text{SO}_4$  as the principal component of the chemical-colored liquor, and produced solar coatings on the stainless steel surface. This coatings were direct reaction between the components in the stainless steel substrate and the chemical-colored solution, changing the traditional way of bonding the coating to the substrate. This method has good coating bonding. We analyzed the elemental composition and surface morphology of the coatings and studied how they behaved after being heated to a high temperature in air. We discovered that  $PC$  was only 0.0268 when the coatings had been aged for 600 h at a high temperature of  $500\text{ }^\circ\text{C}$  in air;  $PC$  became 0.0595 by the 1000<sup>th</sup> hour. Hence the coatings exhibit excellent stability in high-temperature air.

## 2. Experiment and Test

### 2.1. Sample Preparation

#### 2.1.1. Pretreatment

Ultra-pure ferritic stainless steel [24] was a kind of ferritic stainless steel with ultra-low C and N content (150–250 ppm), low Ni, high Cr (13–30%), and addition of trace Mo and Nb elements. Compared to austenitic stainless steel, ultra-pure ferritic stainless steel applications in solar applications have very great advantages, such as higher thermal conductivity (130% to 150%), high corrosion resistance, lower tendency to process hardening, etc. TTS445J1 is a typical steel grade of ultra-pure ferritic stainless steel, and its chemical composition is shown in Table 1. TS445J1 stainless steel is adopted as the matrix for our samples with dimensions  $100\text{ mm} \times 100\text{ mm} \times 0.41\text{ mm}$ . The stainless steel surface needs to be rinsed before treatment as there exist greasy dirt, floating dusts, and other impurities. The sample surface was cleaned up through two procedures, acid pickling and water washing, in this experiment. The pickling solution is composed of 0.54 g/L  $\text{HNO}_3$  and 0.27 g/L DIPSOL ST-305 ( $\text{NH}_4\text{HF}_2 + \text{NaHF}_2$ ), with the solvent being tap water.

**Table 1.** Chemical composition of tested materials ( $\omega/\%$ ).

Specimens	Cr	Mo	Ti	Nb	C	N	S	P	Fe
TTS445J1	30	2	0.05	0.05	0.0021	0.0008	0.0021	0.006	Bal.

At room temperature, the stainless steel samples are immersed into the pickling solution for 30 s and then water-washed for 30 s each of three times to effectively eliminate the greasy dirt, impurities and the pickling solution from the sample surface. Alongside surface cleaning during the acid pickling procedure, the sample surface also undergoes

activating treatment by acid-etching the originally compact stainless steel surface to form a nanoscale cellular structure to enhance the adhesive force for the chemical-colored coatings.

### 2.1.2. Preparation of the Absorber Coatings

TTS445J1 stainless steel is predominated by Fe and Cr elements, as well as trace contents of Mo, Ti, Nb, and other elements. The element components have chemical reactions with the principal coloring liquor of  $\text{Na}_2\text{Cr}_2\text{O}_7\text{-H}_2\text{SO}_4$ , forming a coatings on the stainless steel surface.  $\text{Na}_2\text{Cr}_2\text{O}_7\text{-H}_2\text{SO}_4$  is the main component of the dichromate method [25] in the colored stainless steel process, and by adding different additives and stabilizers, the desired composition and color of the coating has been reached. The metal components such as Fe and Cr in stainless steel are oxidized in  $\text{H}_2\text{SO}_4$  to form anodes. The anode will undergo a reduction reaction with  $\text{Na}_2\text{Cr}_2\text{O}_7$  and  $\text{Cr}^{6+}$  will become  $\text{Cr}^{3+}$ , which in turn will form a Cr-Fe composite oxide with the element O. The semiconductor properties of the Cr-Fe composite oxide are the basis for the spectral selectivity. The chemical-colored liquor whose principal component is  $\text{Na}_2\text{Cr}_2\text{O}_7\text{-H}_2\text{SO}_4$  is added with stabilizers  $\text{Fe}_2(\text{SO}_4)_3$  and  $\text{Cr}_2(\text{SO}_4)_3$ . Compositions of the coloring liquor are 10.7 g/L  $\text{Na}_2\text{Cr}_2\text{O}_7$ , 17.9 g/L  $\text{H}_2\text{SO}_4$ , 0.13 g/L  $\text{Fe}_2(\text{SO}_4)_3$ , and 0.13 g/L  $\text{Cr}_2(\text{SO}_4)_3$ . The chemical-colored liquor is warmed in a constant-temperature (118 °C) heating trough. During the coloring process, an electrochemical workstation is adopted to record the coloring potential and reaction time and plot coloring potential—time curves, with the stainless steel sample as the cathode and the reference electrode Pt as the anode. For ultrapure ferrite steels, in the new technology of chemical-colored of stainless steel, the coloring potential difference is selected within 17.9 mV~19.1 mV, preferred at 18.4 mV, and the coloring reaction time is selected as 560 s. After the coloring reaction, the samples are taken out and water-washed for 30 s each of three times to effectively remove the coloring liquor from their surface, and then dried in a blast drying oven.

### 2.2. Durability Experiment in High-Temperature Air

An intelligent muffle furnace (Sx2-12-12, Shanghai Xin Yi Instruments and Meters Co., Ltd.) is adopted for a high-temperature durability experiment on the fabricated Cr-Fe composite oxide coatings. In the experiment the starting temperature was 25 °C, the rate of temperature rise/drop was  $\pm 20$  °C/min, and heat preservation uniformity was  $\pm 5$  °C. Upon reaching the specified temperature test deadline, the samples cooled naturally before corresponding performance characterization.

There remains no uniform executive standard for high-temperature aging acceleration experiments on medium-to-high-temperature SSACs. We referred to the Chinese national energy industry standard “Medium Temperature Vacuum Solar Absorbing coatings” (NB/T 34048-2017) for relevant provisions on high temperature tolerance rating of medium-temperature vacuum absorbing coatings. This standard provides that the test temperature be 450 °C in vacuum environment (twice the stagnation temperature) and that the test duration be 200 h ( $PC \leq 0.05$ , simulated lifetime 25 years). We aged the fabricated coatings at high temperature, with the test temperature designed to be twice (500 °C) the maximum working temperature (250 °C) of medium temperatures. The test durations were 200 h, 400 h, 600 h, and 1000 h. Finally, the samples cooled naturally before undergoing the corresponding performance characterization test.

### 2.3. Experimental Results Characterization

A scanning electron microscope (SEM) (JEOL, JEM-2010, Tokyo, Japan) is adopted for coatings surface and cross-section morphology analysis. Energy disperse spectroscopy (EDS) is adopted for component analysis of all regions of the coatings at acceleration voltage 1~15 kV. The ultraviolet-visible-infrared spectrophotometer (Shimadzu, UV-3600, Kyoto, Japan) of an integrating sphere is equipped to measure the spectral reflectance  $R(\lambda)$  of the samples, and the reflectivity spectra of the coatings are measured against the AM1.5 reference spectrum at room temperature within a wavelength range of 300 nm~2400 nm.

The baseline sample BaSO<sub>4</sub> is adopted for correction at a resolution of 1 nm. The solar absorptance ( $\alpha$ ) is calculated by formulae (2) and (3). The Fourier transform infrared spectrophotometer (Shimadzu, IR-Affinity-1, Kyoto, Japan) was used to characterize the thermal reflectance of coatings. FTIR was operated with a Fourier transform infrared fiber optic device that measures the laser-generated interferogram and outputs it as a sinusoidal signal of the laser wavelength amplitude. The coating spectral directional reflectance  $R_{\lambda}^{SP}$  was characterized by FTIR at an incidence angle of 8° with a variable angle reflection attachment in the wave number is 4000~400 cm<sup>-1</sup> (250~2500 nm) at 90 °C, with a wave number of 4 cm<sup>-1</sup>. The visible and near-infrared reflectance (i.e., 0.25 μm < λ < 1 μm) was measured by a Si detector, while the mid-infrared measurements (i.e., 1 μm < λ < 25 μm) were performed with a deuterated triglyceride sulfate (DTGS) detector. Each measured spectrum was averaged from 32 scans with an aluminum mirror as reference, and the measured reflectance was corrected by the theoretical reflectance of Al. The thermal emittance ( $\epsilon$ ) is calculated by Formula (4).

$$\rho = \frac{\int_{300}^{2400} E_{\lambda} \bullet \rho(\lambda) d\lambda}{\int_{300}^{2400} E_{\lambda} d\lambda} \approx \frac{\sum_{300}^{2400} E_{\lambda} \bullet \rho(\lambda) \Delta\lambda}{\sum_{300}^{2400} E_{\lambda} \Delta\lambda} \quad (2)$$

$$\alpha = 1 - \rho \quad (3)$$

$$\epsilon = \frac{\int_{250}^{2500} [1 - R(\lambda)] P_B(\lambda) d\lambda}{\int_{250}^{2500} [1 - R(\lambda)] P_B(\lambda) d\lambda} \quad (4)$$

where  $\rho$  is the solar emission,  $\rho(\lambda)$  is the spectral emission,  $E_{\lambda}$  is the mean value of solar spectral irradiance, W·m<sup>-2</sup>·μm<sup>-2</sup>,  $\lambda$  is the wavelength, nm,  $P_B(\lambda)$  is the Planck's blackbody radiation spectrum,  $R(\lambda)$  is the spectral reflectance,  $P_{\text{sum}}(\lambda)$  is the spectral radiance of AM1.5.

### 3. Experimental Results and Discussions

#### 3.1. Consistence of Optical Performance of the Fabricated Coatings

Consistence of sample performance is a key index for evaluating the validity of a novel technology. With the technological conditions in Section 2.1.2 adopted, five sheets (No. 1–5) of samples were placed in the coloring trough, as shown in Table 2. The samples underwent an optical performance test, and statistics were made, after coloring. The mean of solar absorptances ( $\alpha$ ) is 93.34, with a standard deviation of 0.15%, and the mean of thermal emittance ( $\epsilon$ ) is 13.26, with a standard deviation of 0.79%. From the standard deviations, the consistence of optical performance of the sample coatings meets the general requirements of the experiment, showing this technology has good repeatability.  $\alpha/\epsilon$  is an index reflecting the spectral selectivity of SSACs. Coatings fabricated at the same technological conditions have  $\alpha/\epsilon$  ranging within 6.61~7.74, exhibiting excellent spectral selectivity.

**Table 2.** Optical performance of the initial samples.

No.	Solar Absorptance (AM1.5)	Thermal Emittance (90 °C)	Spectral Selectivity ( $\alpha/\epsilon$ )
1	0.9343	0.1331	7.02
2	0.9312	0.1309	7.11
3	0.9334	0.1206	7.74
4	0.9328	0.1371	6.80
5	0.9352	0.1415	6.61
Average value	0.9334	0.1326	7.04
Standard deviation $\sigma$	0.15%	0.79%	-

### 3.2. Optical Performance of the Coatings through High-Temperature Aging

As seen in Figure 1, the coatings form at 300–1100 nm with broad spectrum absorption. Due to the interference of light, the coatings appeared as blue-black. Thermal stability of coatings is evaluated by heating coatings for long hours in high-temperature (500 °C) air. Figure 1 shows the variations in optical performance of the coatings with respect to distinct high-temperature aging hours. Figure 1a is the reflection spectrogram of the coatings after high-temperature accelerated aging. From spectral reflectance, the reflectivity curves of the coatings show a slight downtrend within the visible spectrum of 300 nm~700 nm, with a subsequent adhesion, indicating that the Cr-Fe composite oxide coatings exhibit extremely high thermal stability within this waveband. Within the waveband of 700 nm~2500 nm, the reflectivity curves of the coatings show an overall uptrend, indicating that the thermal emittance of the coatings would go up in the infrared band. In terms of optical performance, while the coatings are aged at high temperature (500 °C) for less than 800 h,  $\alpha$  changes from 0.9343 to 0.9062, with a lower rate of decay; for 800~1000 h, however,  $\alpha$  has a higher rate of decay.

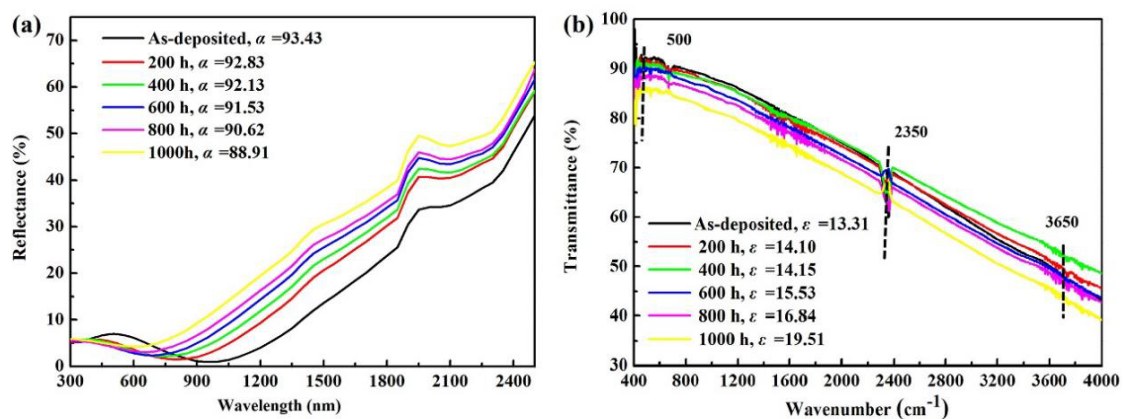


**Figure 1.** Variations in optical performance of the coatings after high-temperature aging: (a) Reflection spectrogram of high-temperature durability of the coatings; (b) Thermal transmission spectral changes of high-temperature durability of the coatings.

Figure 1b is the transmission spectrogram of the coatings after distinct aging hours at high temperature (500 °C) and presents the variation of thermal emittance of the reacting coatings at 90 °C. It is observed that the characteristic stretching vibration peak and bending vibration peak of the Fe-O and Fe-O-H keys of the spinel structure are displayed near the wave numbers 500  $\text{cm}^{-1}$ , 2350  $\text{cm}^{-1}$ , and 3650  $\text{cm}^{-1}$ , showing that the coatings composition is predominated by oxidated compounds of Fe. Meanwhile, the stretching vibration peak and bending vibration peak have changed little with the extension of aging hours, indicating that the coatings material has stable compositions and exhibits excellent thermal stability. In terms of optical performance, the thermal emittance of the coatings rises with the extension of aging hours:  $\epsilon$  increases from the initial 0.1331 to 0.1684 for less than 800 h, and grows rapidly to 0.1951 for aging hours of 800~1000 h.

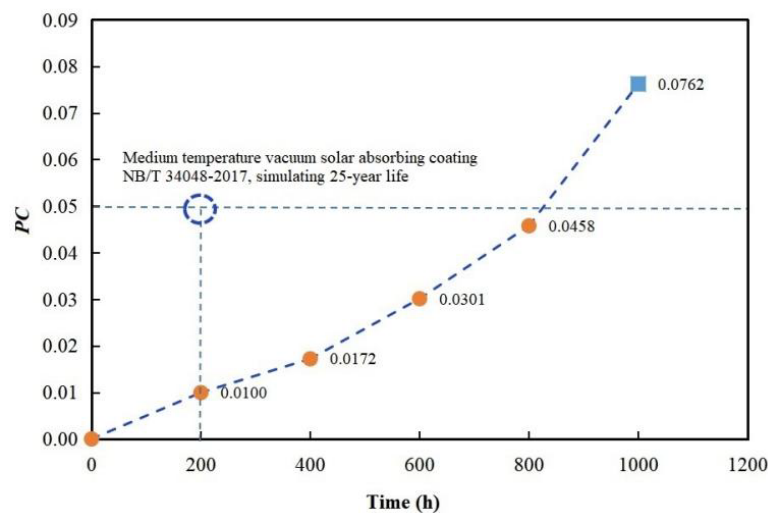
### 3.3. Performance Decay Coefficient of the Coatings through High-Temperature Aging

Table 3 is a statistical table of high-temperature aging optical performance of the Cr-Fe composite oxide coatings. Figure 2 is a scatter plot of  $PC$  after the Cr-Fe composite oxide coatings underwent high-temperature (500 °C) accelerated aging. It is observed that as the coatings are aged at high temperature,  $PC$  bears an approximately linearly incremental relation to time, but that  $PC$  decays to a largening extent after 800 h. By the provisions on high temperature tolerance rating of medium-temperature vacuum absorbing coatings in the Chinese national energy industry standard “Medium temperature vacuum solar absorbing coatings” (NB/T 34048-2017),  $PC \leq 0.05$  and simulated lifetime of coatings is

25 years after 200 h of high-temperature (450 °C) in vacuum environment.  $PC = 0.01$  when the Cr-Fe composite oxide coatings had been aged for 200 h in high-temperature (500 °C) air. Albeit no equivalent relation has been built between the temperature of high-temperature aging in vacuum and that in air, the fact that  $PC = 0.0458$  by the 800th hour of aging of the Cr-Fe composite oxide coatings remains a piece of evidence that such Cr-Fe composite oxide coatings produced by the new technology of chemical-colored have a lifetime exceeding 25 years.

**Table 3.** High-temperature durability test on the coatings.

Optical Properties of the Coatings		$t_1 = 200$ h	$t_2 = 400$ h	$t_3 = 600$ h	$t_4 = 800$ h	$t_5 = 1000$ h
$\alpha$	0.9343	0.9283	0.9213	0.9153	0.9062	0.8891
$\varepsilon$ (90 °C)	0.1331	0.1410	0.1415	0.1553	0.1684	0.1951
$PC$		0.0100	0.0172	0.0301	0.0458	0.0762



**Figure 2.** Distribution of  $PC$  with time in the high-temperature (500 °C) durability experiment.

### 3.4. Morphology Analysis of the Coatings through High-Temperature Aging

Figure 3 is a set of surface and cross-section SEM graphs of the coatings before and after high-temperature (500 °C) aging for 1000 h. Clearly, Figure 3a,c display the coatings in the initial state consist of regular arrangement of columnar grains with a diameter of about 5 nm. The grains were generally smooth and neat, and the coating thickness was about 450 nm. The grain compactness was gradually tightened along the substrate towards the coating surface. However, the grain interfaces are loosely aligned in some regions, which could cause certain defects in the coatings surface. Combined with Figure 1, the emission spectrum trend and the Fe-O and Fe-O-H of the transmission spectra are basically unchanged, indicating that the coatings compositions have changed slightly, while the change in optical performance has been caused mainly by the coatings surface morphology change. Figure 3b,d display the grain growth on the surface after high-temperature accelerated aging. A stress has been engendered around large-sized grains, breaking the original alignment of grains. Grain alignment has been disordered in different patterns, leading to coatings surface morphology reconstruction, which is another reason for the great variation of thermal emittance of the coatings. The coatings surface morphology reconstruction may also be ascribed to the disparity between the coefficients of thermal expansion of the stainless steel base material and the coatings, such that the coatings surface defects have given rise to cracks. After thermal treatment for a long time at high-temperature condition, oxygen would reach the surface of the matrix through cracks, thereby oxidating the substrate and generating an oxide layer, leading emissivity to further

increase. Comparison of Figure 3c,d, it can be found that the substrate grain size and arrangement did not change, indicating that the stainless steel substrate resistance to oxidation. At the same time, the phenomenon of coatings grain growth, only in the area close to the substrate, the coatings surface grain size does not change much. We speculate that the surface morphology reconstruction was not strong. The surface morphology reconstruction, which increases the coatings thermal emittance, but also increases the optical trap depth and improves the solar absorbance. Finally, the coating-substrate interface does not change significantly and exhibits a high coating bond.

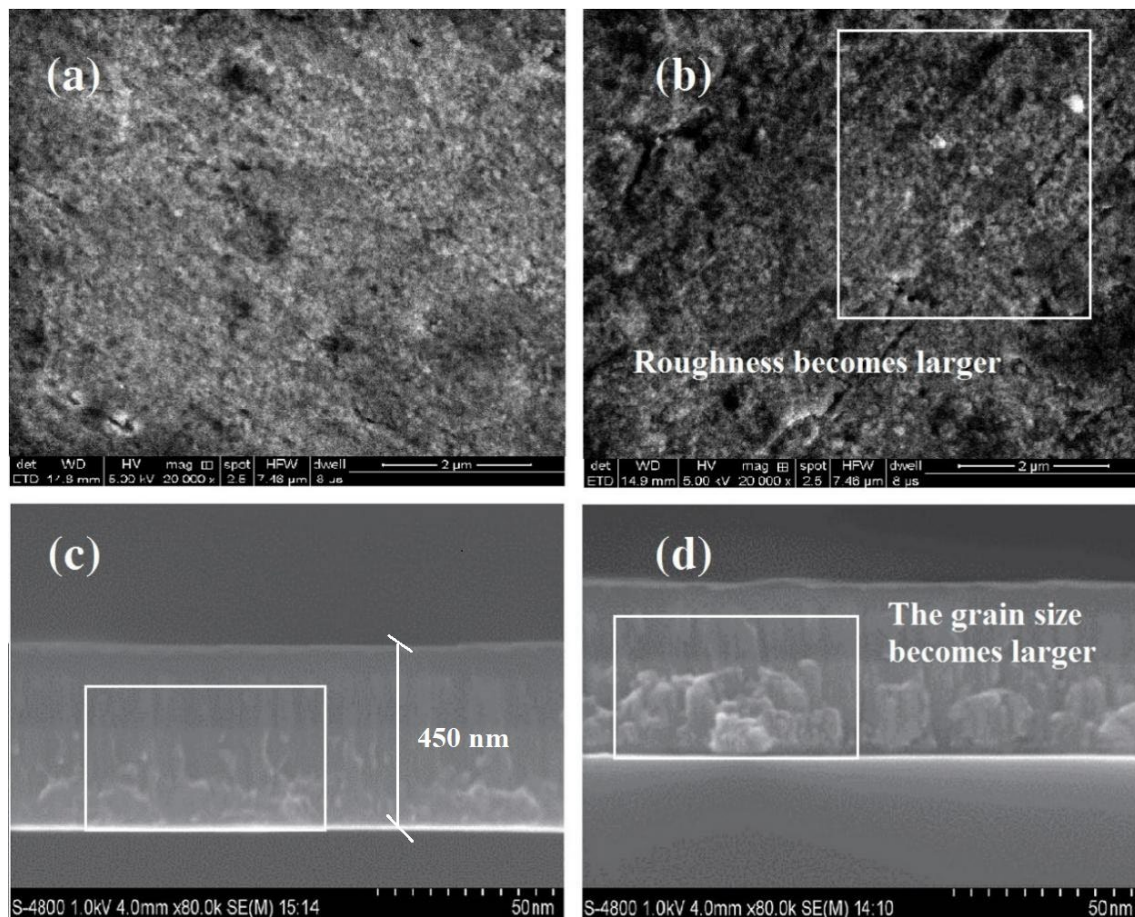


**Figure 3.** Surface and cross-section morphologies of the coatings before and after high-temperature aging (500 °C, 1000 h): (a) surface morphology of the coatings before aging; (b) surface morphology of the coatings after aging; (c) cross-sectional morphology of the coatings before aging; (d) cross-sectional morphology of the coatings before aging.

### 3.5. Composition and Phase Components of the Coatings through High-Temperature Aging

Figure 4 presents the EDS energy spectra of the coatings before and after high-temperature aging for 1000 h. Analysis of the selected regions of the coatings with high temperature aging showed that the positions and atomic percentages of the characteristic peaks of Fe, Cr, and O were unchanged. In particular, the slight change in the O atomic percentage indicates the high oxidation resistance of the material in the coatings. This phenomenon indicates that the physical phase composition of the Cr-Fe oxide complex remains stable after the coatings were aged in high temperature air at 500 °C for up to 1000 h, which shows the good thermal stability of the coatings. However, comparing Figure 4 Mo variation, due to the extremely low content of Mo element in TTS445J1. We speculate that equipment errors or miscellaneous summits mask the accurate characterization of Mo elements.

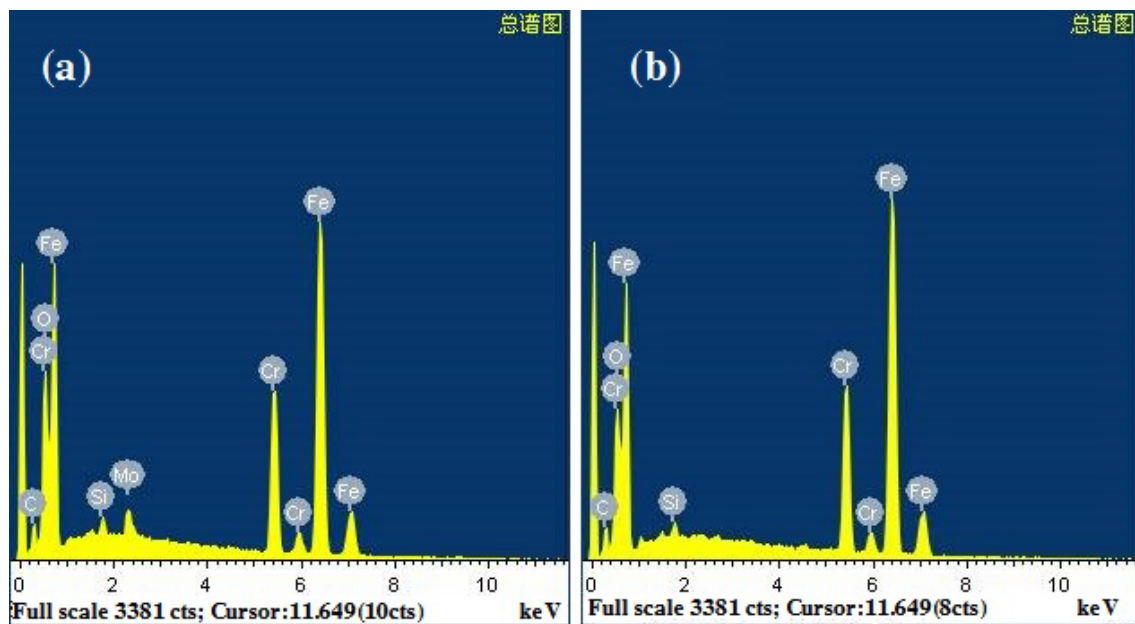


**Figure 4.** EDS energy spectrum analysis of the coatings: (a) The original state of the coatings; (b) high-temperature (500 °C) aging for 1000 h.

The coatings have been produced by chemically coloring the stainless steel base material, and they are relatively thin and hard to peel off. For several times, we conducted further analysis into the composition and phase structures and composite oxide contents of the coatings by XRD and XPS. Since the principal component of stainless steel is the Fe element, the diffraction peak is high above those of other compounds. A big pity is that we failed to acquire the precise composition and phase structures of composite oxides of the coatings. Nevertheless, combined with the transmission spectra of the coatings in Figure 1, the cross-section SEM in Figure 3 and other studies on stainless steel chemical coloration, it can be determined that the coatings Cr-Fe composite oxides with a spinel structure.

According to the experimental analysis, the aging of Cr-Fe composite oxides in high-temperature air basically abides by the principle of electron transition with high-temperature aging of thin films. While the stainless steel base material is undergoing chemical-colored, the atomic configuration inside the Cr-Fe composite oxides forming on the stainless steel surface goes out of order, leading to the loose alignment of local grain interfaces and certain defects in the coatings surface. At the initial stage of high-temperature aging, the loss of H<sub>2</sub>O molecules from the hydrates in the coatings causes the grains to largen, so that the variation of  $\alpha$  of the coatings is significant. This explains the variation trend of spectral reflectance of the coatings in Figure 1a. With the extension of aging hours, grains of the coatings largen, creating a large number of segregated atoms and vacancies. The atoms gain an increasing energy at high temperature and deviate from their original position, forming a fast channel for atomic diffusion, and giving rise to slight reconstruction of coatings surface morphology. This point is demonstrated in Figure 3b,d. The composition and phase structures and components of Cr-Fe composite oxides in the coatings are relatively stable, but the coatings surface morphology reconstruction is manifested in optical performance as the fact that the emission spectrum and transmission spectrum trends of the coatings are basically unchanged, and that the thermal emittance of the coatings decays more significantly than solar absorptance.

#### 4. Conclusions

In this work, we have adopted TTS445J1 stainless steel as the base material and Na<sub>2</sub>Cr<sub>2</sub>O<sub>7</sub>-H<sub>2</sub>SO<sub>4</sub> as the principal coloring liquor and performed chemical-colored at certain temperature to produce the photothermal coatings, which have excellent repeatability

of process and a prospect of extensive applicability. The coatings have good spectral selectivity,  $\alpha/\varepsilon = 0.9334/0.1326$ , and the thickness of the coatings was about 450 nm. The chromium-iron composite oxide coatings with spinel structure were obtained by the chemical-colored of the stainless steel, which was obtained by the direct reaction between the stainless steel substrate and the chemical-colored solution. This method changed the traditional coating and substrate physical bonding method. After high-temperature aging, we did not find that the coatings and substrates occur obvious interface diffusion, indicating that this method has good coating bonding. At the same time, the stainless steel substrate grains did not change, indicating that the substrate also has good resistance to oxidation after the reaction. Finally, the structure of the Cr-Fe composite oxide materials were stable when the coatings were aged at 500 °C in air for up to 1000 h. The thermal stability of the coatings were assessed by heating at 500 °C in air, aging for 200 h, PC was 0.01, after 800 h high temperature aging, PC was 0.0458, aging time was extended to 1000 h, PC was 0.0762. The optical properties of the coatings decayed due to the loss of water molecules from the hydrate components in the coatings resulting in larger grains, which in turn affected the slight reconstruction of the surface morphology of the coatings.

**Author Contributions:** Conceptualization, H.Y.; Writing-review & editing, H.Y.; Writing-original draft, Y.H.; Formal analysis, Z.S.; Data curation, X.Z.; Supervision, Y.X.; Resources, L.F. All authors have read and agreed to the published version of the manuscript.

**Funding:** This research received no external funding.

**Data Availability Statement:** Data are contained within the article.

**Acknowledgments:** This work was supported by the Opening Funds of State Key Laboratory of Building Safety and Built Environment & National Engineering Research Center of Building Technology (No. BSBE2020-10), Natural Science Foundation of Shandong Province (No. ZR2020KE020, ZR2021ME185), Science and Technology SMEs Innovation Capacity Enhancement Project of Shandong Province (No. 2022TSGC2144, 2022TSGC2322).

**Conflicts of Interest:** The authors declare no conflict of interest.

## References

1. Islam, M.T.; Huda, N.; Abdullah, A.B.; Saidur, R. A comprehensive review of state-of-the-art concentrating solar power (CSP) technologies: Current status and research trends. *Renew. Sustain. Energy Rev.* **2018**, *91*, 987–1018. [[CrossRef](#)]
2. Mekhilef, S.; Saidur, R.; Safari, A. A review on solar energy use in industries. *Renew. Sustain. Energy Rev.* **2011**, *15*, 1777–1790. [[CrossRef](#)]
3. Schnitzer, H.; Brunner, C.; Gwehenberger, G. Minimizing greenhouse gas emissions through the application of solar thermal energy in industrial processes. *J. Clean. Prod.* **2007**, *15*, 1271–1286. [[CrossRef](#)]
4. Wu, S.; Cheng, C.-H.; Hsiao, Y.-J.; Juang, R.-C.; Wen, W.-F. Fe<sub>2</sub>O<sub>3</sub> films on stainless steel for solar absorbers. *Renew. Sustain. Energy Rev.* **2016**, *58*, 574–580. [[CrossRef](#)]
5. Joshi, R.; Chhibber, R. High temperature wettability studies for development of unmatched glass-metal joints in solar receiver tube. *Renew. Energy* **2018**, *119*, 282–289. [[CrossRef](#)]
6. Carling-Plaza, A.; Muhammad, A.K.; Maxime, B.; Audrey, S.-G.; Laurent, T.; Laurent, D. Demonstration of long term stability in air at high temperature for TiAlN solar selective absorber coatings. *AIP Conf. Proc.* **2019**, *2126*, 030026.
7. Sibin, K.P.; John, S.; Barshilia, H.C. Control of thermal emittance of stainless steel using sputtered tungsten thin films for solar thermal power applications. *Sol. Energy Mater. Sol. Cells* **2015**, *133*, 1–7. [[CrossRef](#)]
8. Lee, D.B.; Nguyen, T.D.; Kim, S.K. Air-oxidation of nano-multilayered CrAlSiN thin films between 800 and 1000 °C. *Surf. Coat. Technol.* **2009**, *203*, 1199–1204. [[CrossRef](#)]
9. Lu, B.; Peng, Y.; Ren, T.; Yao, H.; Wang, Y.; Liu, H.; Zhu, Y. Preparation and thermal stability of a novel mid-temperature air-stable solar selective coating. *Appl. Surf. Sci.* **2019**, *487*, 840–847. [[CrossRef](#)]
10. Yang, Z.; Tan, S.; Yang, J.; Li, Y.; Yang, X.; Deng, J. Study on the solar selectivity and air thermal stability of cobalt–nickel–iron oxide coating fabricated by spraying method. *Opt. Mater.* **2021**, *111*, 110573. [[CrossRef](#)]
11. Niranjana, K.; Soum-Glaude, A.; Carling-Plaza, A.; Bysakh, S.; John, S.; Barshilia, H.C. Extremely high temperature stable nanometric scale multilayer spectrally selective absorber coating: Emissivity measurements at elevated temperatures and a comprehensive study on ageing mechanism. *Sol. Energy Mater. Sol. Cells* **2021**, *221*, 110905. [[CrossRef](#)]
12. Elton, D.N.; Arunachala, U.C. Parabolic Trough Solar Collector for Medium Temperature Applications: An Experimental Analysis of the Efficiency and Length Optimization by Using Inserts. *J. Sol. Energy Eng.* **2018**, *140*, 061012. [[CrossRef](#)]

13. Venkatalaxmi, A.; Padmavathi, B.S.; Amaranath, T. A general solution of unsteady Stokes equations. *Fluid Dyn. Res.* **2004**, *35*, 229–236. [[CrossRef](#)]
14. Randich, E.; Allred, D.D. Chemically vapor-deposited ZrB<sub>2</sub> as a selective solar absorber. *Thin Solid Film.* **1981**, *83*, 393–398. [[CrossRef](#)]
15. Liu, H.D.; Yang, B.; Mao, M.R.; Liu, Y.; Chen, Y.M.; Cai, Y.; Fu, D.J.; Ren, F.; Wan, Q.; Hu, X.J. Enhanced thermal stability of solar selective absorber based on nano-multilayered TiAlON films deposited by cathodic arc evaporation. *Appl. Surf. Sci.* **2020**, *501*, 144025. [[CrossRef](#)]
16. Anastasiou, E.; Lorentz, K.O.; Stein, G.J.; Mitchell, P.D. Prehistoric schistosomiasis parasite found in the Middle East. *Lancet Infect. Dis.* **2014**, *14*, 553–554. [[CrossRef](#)]
17. AL-Rjoub, A.; Rebouta, L.; Costa, P.; Vieira, L.G. Multi-layer solar selective absorber coatings based on W/WSiAlN<sub>x</sub>/WSiAlO<sub>y</sub>N<sub>x</sub>/SiAlO<sub>x</sub> for high temperature applications. *Sol. Energy Mater. Sol. Cells* **2018**, *186*, 300–308. [[CrossRef](#)]
18. Torres, J.F.; Tsuda, K.; Murakami, Y.; Guo, Y.; Hosseini, S.; Asselineau, C.-A.; Taheri, M.; Drewes, K.; Tricoli, A.; Lipiński, W.; et al. Highly efficient and durable solar thermal energy harvesting via scalable hierarchical coatings inspired by stony corals. *Energy Environ. Sci.* **2022**, *15*, 1893–1906. [[CrossRef](#)]
19. Wang, H.; Alshehri, H.; Su, H.; Wang, L. Design, fabrication and optical characterizations of large-area lithography-free ultrathin multilayer selective solar coatings with excellent thermal stability in air. *Sol. Energy Mater. Sol. Cells* **2018**, *174*, 445–452. [[CrossRef](#)]
20. Prasad, M.S.; Mallikarjun, B.; Ramakrishna, M.; Joarder, J.; Sobha, B.; Sakthivel, S. Zirconia nanoparticles embedded spinel selective absorber coating for high performance in open atmospheric condition. *Sol. Energy Mater. Sol. Cells* **2018**, *174*, 423–432. [[CrossRef](#)]
21. Atchuta, S.R.; Sakthivel, S.; Barshilia, H.C. Transition metal based CuxNiyCoz-x-yO4 spinel composite solar selective absorber coatings for concentrated solar thermal applications. *Sol. Energy Mater. Sol. Cells* **2019**, *189*, 226–232. [[CrossRef](#)]
22. Dutra, K.H.; Freire, F.N.A.; Pinho, D.C.; Araújo, F.A.A. Characterization of a Selective Surface Based on Chromium, Iron and Aluminum Oxides for Application in Solar-Thermal Collectors. *Mater. Res.* **2022**, *25*, e20210489. [[CrossRef](#)]
23. Corredor, J.; Bergmann, C.P.; Pereira, M.; Dick, L.F.P. Coloring ferritic stainless steel by an electrochemical–photochemical process under visible light illumination. *Surf. Coat. Technol.* **2014**, *245*, 125–132. [[CrossRef](#)]
24. Yangyang, Z.; Likui, N.; Chaohui, D. Effects of Ti-Nb Microalloying on the Microstructure and Mechanical Properties of Ultra-pure 30% Cr Super Ferritic Stainless Steel. *Rare Met. Mater. Eng.* **2022**, *51*, 1845–1856.
25. Fan, C.; Shi, J.; Sharafiev, A.; Lemmens, P.; Dilger, K. Optical spectroscopic and electrochemical characterization of oxide films on a ferritic stainless steel. *Mater. Corros.* **2020**, *71*, 440–450. [[CrossRef](#)]

**Disclaimer/Publisher’s Note:** The statements, opinions and data contained in all publications are solely those of the individual author(s) and contributor(s) and not of MDPI and/or the editor(s). MDPI and/or the editor(s) disclaim responsibility for any injury to people or property resulting from any ideas, methods, instructions or products referred to in the content.